Ignition probability of polymer-bonded explosives accounting for multiple sources of material stochasticity

S. Kim, A. Barua, Y. Horie, and M. Zhou

Citation: Journal of Applied Physics **115**, 174902 (2014); doi: 10.1063/1.4874915
View online: http://dx.doi.org/10.1063/1.4874915
View Table of Contents: http://scitation.aip.org/content/aip/journal/jap/115/17?ver=pdfcov
Published by the AIP Publishing

Ignition probability of polymer-bonded explosives accounting for multiple sources of material stochasticity

S. Kim,[1] A. Barua,[1] Y. Horie,[2] and M. Zhou[1,a)]
[1]*The George W. Woodruff School of Mechanical Engineering, Georgia Institute of Technology, Atlanta, Georgia 30332-0405, USA*
[2]*(ret.) Air Force Research Lab, Munitions Directorate, 2306 Perimeter Road, Eglin AFB, Florida 32542, USA*

(Received 18 February 2014; accepted 11 April 2014; published online 2 May 2014)

Accounting for the combined effect of multiple sources of stochasticity in material attributes, we develop an approach that computationally predicts the probability of ignition of polymer-bonded explosives (PBXs) under impact loading. The probabilistic nature of the specific ignition processes is assumed to arise from two sources of stochasticity. The first source involves random variations in material microstructural morphology; the second source involves random fluctuations in grain-binder interfacial bonding strength. The effect of the first source of stochasticity is analyzed with multiple sets of statistically similar microstructures and constant interfacial bonding strength. Subsequently, each of the microstructures in the multiple sets is assigned multiple instantiations of randomly varying grain-binder interfacial strengths to analyze the effect of the second source of stochasticity. Critical hotspot size-temperature states reaching the threshold for ignition are calculated through finite element simulations that explicitly account for microstructure and bulk and interfacial dissipation to quantify the time to criticality (t_c) of individual samples, allowing the probability distribution of the time to criticality that results from each source of stochastic variation for a material to be analyzed. Two probability superposition models are considered to combine the effects of the multiple sources of stochasticity. The first is a parallel and series combination model, and the second is a nested probability function model. Results show that the nested Weibull distribution provides an accurate description of the combined ignition probability. The approach developed here represents a general framework for analyzing the stochasticity in the material behavior that arises out of multiple types of uncertainty associated with the structure, design, synthesis and processing of materials. [http://dx.doi.org/10.1063/1.4874915]

I. INTRODUCTION

Polymer-bonded explosives (PBXs) consist of solid energetic materials and a polymer binder. Because the safety in the handling of explosives and the vulnerability to accidental stimuli relate to the sensitivity of the materials,[1] researchers have shown increased interest in the sensitivity, but the mechanisms of solid high explosives' reactivity are intricate and still not well understood,[2] particularly in the case of non-shock ignition by impact loading such as that seen in drop weight and Susan tests. To establish a basic understanding of impact sensitivity, this paper continues our effort over the last few years[3–7] towards the goal of moving the study of impact sensitivity from empiricism based on protocols to design science based on modeling and simulation that capture underlying physics.

The initiation of high explosives under impact loading is governed by hotspots created by localized mechanical energy dissipation. Relevant mechanisms of energy dissipation include void collapse, plasticity, frictional heating between particles, and heating at crack tips.[8] These mechanisms are heavily influenced by such factors as material heterogeneity, constituent properties, and defects. The nature of these influences causes the ignition process to be fundamentally stochastic. Recognizing this reality, researchers have carried out numerous studies pertaining to this topic. For example, Dienes *et al.* conducted pioneering studies on impact ignition through the statistical modeling of microcracking and frictional heating.[9–11] Nichols and Tarver[12] used statistical hotspot models and investigated the effects of pressure, hotspot size, and hotspot number density. Hamate *et al.*[13] developed a mechanical reactive burn model using a statistical approach of hotspot evolution. These studies provide an understanding of effects of cracks or hotspot characteristics on initiation using analytical models of crack growth or hotspot aggregation. However, the effects of randomly distributed inhomogeneities and corresponding initiation probability of explosives remain to be quantified.

Probabilistic approaches have long been used to study the mechanical behavior of materials with randomly distributed defects. For example, Hassold *et al.*[14] used the Weibull distribution and the Gumbel distribution (a double exponential form of the Weibull distribution) to analyze the effects of defect density, domain size, and spring modulus on the probability of failure. The idealized structures consist of springs with random defects. Using the Weibull and modified Gumbel distributions, Duxbury *et al.*[15] analyzed the failure probability of idealized structures comprised of fiber bundles with random defects. Andersons *et al.*[16] performed tension tests on fibers with random defects and obtained the distribution of strengths. With regard to the effect of random

a)Electronic mail: min.zhou@me.gatech.edu

material properties, Silberschmidt *et al.*[17] studied stochastic crack propagation in brittle materials with spatially random variations of stiffness. These studies show that random defects and the fluctuations of material properties are primary sources for stochasticity in material response.

In composite materials, interactions between two different phases cause the following issues that single-phase materials do not have. One key factor that dominates the fracture in composites is the interfacial strength between constituents. Studies[18–21] have highlighted the effects of debonding of particle/matrix interfaces in composites. Yanase *et al.*[22] developed a constitutive model that relates the discontinuity of displacements to traction for the quasi-static deformation of composites, accounting for the effect of imperfect particle-binder interfaces. Another key factor in composite material is its inherent random morphology of different phases. Ostoja-Starzewski[23] used randomly distributed and periodically distributed fibers in composites, and performed numerical analysis to determine how the effective elastic moduli, the effective constitutive response, and the geometric patterns of damage change. Vel and Goupee[24,25] analyzed the effects of the random microstructural morphology of two-phase composites on material properties such as Young's modulus, the thermal expansion coefficient, and principal stresses at failure in tension and compression.

In most cases however, as Freudenthal describes,[26] "inhomogeneity expressed in the form of the statistical scatter of observed characteristics is the result of both the submicroscopic defects and the macroscopic random inhomogeneities in the material." Obviously, the uncertainty in material behavior is not caused by individual sources of inhomogeneities alone, but rather by the combined effect of multiple factors.

This study recognizes Freudenthal's observation and focuses on the effects of two sources of stochastic variations at the microstructural level on hotspot development in a PBX. The random variations considered are associated with the morphologies of constituent phases and the bonding strength of the grain-binder interfaces. Microstructures with statistically similar properties are generated with variations in the morphologies of the grains and binder and in the interfacial bonding strength between the grains and the binder. The probability of ignition arising from one source of stochastic variation is quantified and analyzed separately from another source. The two probability functions are then combined using relations between the time to criticality and microstructure attributes. The specific mathematical form used is the three-parameter Weibull distribution function.

II. FRAMEWORK OF ANALYSIS

A. Microstructure

The microstructures that this paper analyzes simulate PBX consisting of HMX grains and an Estane binder. Typical shape of energetic grains in the computationally generated microstructure used for the meso-scale simulation is either circular[27,28] or polygonal generated by the Voronoi tessellation method.[7,18] Wu *et al.*[24] showed that simulations of the Brazilian compression test using PBX microstructures generated by the Voronoi tessellation method yield results that match the results of experiments reasonably well. Although the microstructures generated by the Voronoi method have more realistic shapes of grains, they have monomodal size distribution, whereas HMX crystals in PBX9501 have bimodal size distributions.[21]

To obtain microstructures that are similar to PBX9501, we use a grain library with a bimodal grain size distribution. This library consists of grains extracted from microstructures generated by the Voronoi tessellation method. Two microstructures, one with large grains (see Fig. 1(a)) and the other with small grains (see Fig. 1(b)), are generated. The grains in each microstructure are detected and stored separately in the grain library as shown in Fig. 1(c). Finally, grains in the library are randomly distributed on the microstructure domain as seen in Fig. 1(d). To achieve a high packing density, the larger grains ($d > 200\,\mu m$) are initially placed at random locations up to a specified volume fraction (e.g., $\eta = 0.55$–0.60). Subsequently, smaller grains ($d < 200\,\mu m$) are placed between the larger grains, until the desired volume fraction ($\eta = 0.81$) is reached. The time required for generating a micrograph increases with the desired packing density. To reduce the time required in generating micrographs with a high packing density ($\eta > 0.70$), a random shuffling algorithm is employed. Specifically, if a grain cannot be placed in the domain, the locations of the existing grains are randomly altered until an empty region can be found for that particular grain. Naturally, such a method cannot be used indefinitely. There is a packing density beyond which grains can no longer be accommodated. This method is capable of achieving a relatively high packing density of $\eta \sim 0.81$. For the bimodal distributions, the two mean grain sizes are $\sim 123\,\mu m$ and $\sim 289\,\mu m$. The average standard deviation for the smaller size is $37.2\,\mu m$ and the large size is $49.9\,\mu m$.

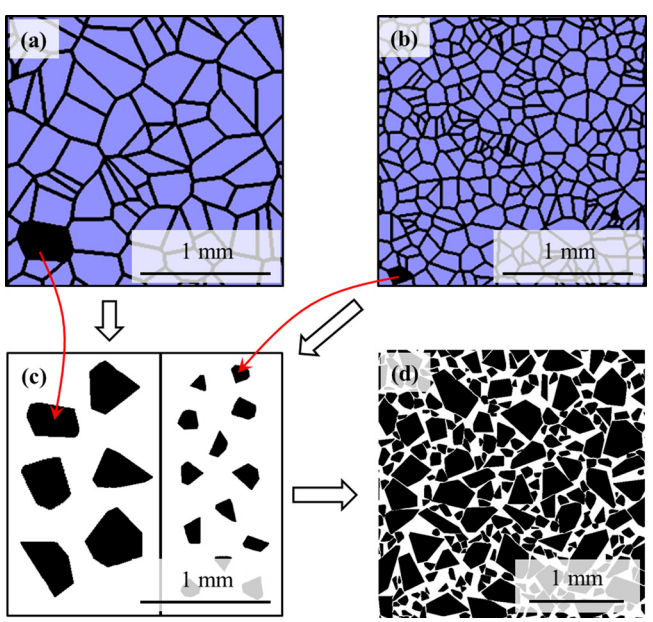

FIG. 1. Generation of microstructures with bimodal size distributions; (a) and (b) Microstructures generated by Voronoi tessellation: (a) with coarse grains and (b) with fine grains; (c) Grain library with coarse and fine grains extracted from the microstructures of Voronoi tessellation; (d) Microstructure with bimodal size grains that are randomly placed.

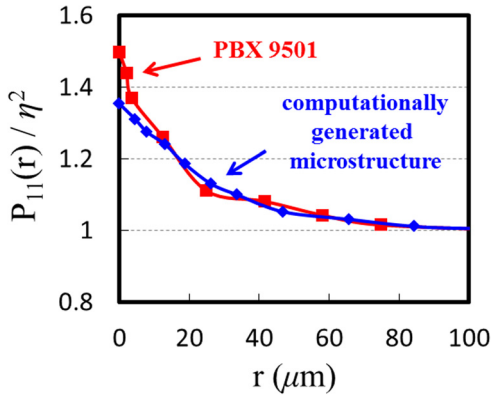

FIG. 2. Comparison of the two-point correlation functions of the microstructure of PBX 9501 (Ref. 28) and computationally generated microstructure.

The evaluation of the computationally generated microstructure is performed by comparing the two-point correlation function of PBX 9501 microstructure and that of computationally generated microstructure. The gray-scale image of the PBX 9501 microstructure ($\eta = 0.70$) was obtained by Liu.[29] The microstructure of PBX 9501 typically includes HMX grains close to 95% by mass fraction (92% by volume fraction). However, as Mas *et al.*[30] observed, some particles are too small to be resolved by micrographs, resulting in less volume fraction than actual PBX9501 is composed of. Figure 2 shows that the two-point correlation function of PBX 9501 microstructure strongly matches that of the computationally generated microstructure ($\eta = 0.74$) from the grain library approach. Multiple microstructures with the same attributes are generated based on the approach described previously. To illustrate the random variations in microstructure morphology, Figure 3 shows five samples with the same packing density of $\eta = 0.81$.

In addition to having variations in constituent morphologies, the microstructures have statistical variations in the bonding strength between the binder and the grains. In modeling, these variations manifest in the maximum traction (S_{max}) of the cohesive relation that determines the strengths of the interfaces in the normal and shear directions. Details of the framework used are given in Barua *et al.*[5]

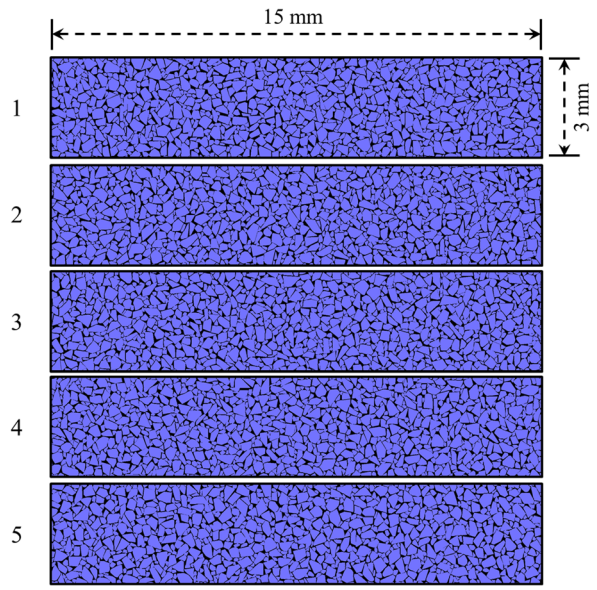

FIG. 3. Multiple samples of computationally generated microstructures with a bimodal grain size distribution and a grain volume fraction of $\eta = 0.81$.

The effect of interfacial bonding strength is analyzed using two microstructure groups. The first group has spatially uniform bonding strengths between the phases but randomly varying phase morphologies. Sample sets in this group have one of six levels of the maximum traction (S_{max} =0.1, 17.5, 35, 70, 100, and 1000 MPa) and each set consists of twenty microstructure samples. This group has a total of $20 \times 6 = 120$ samples. The critical displacement is 4.62 μm for all of the six sets which represent different levels of fracture energy (γ_c) in the range of $0.231 - 2310\,J/m^2$. The maximum traction of 35 MPa corresponds to a fracture energy of $\gamma_c = 81\,J/m^2$ which matches the experimental data in Ref. 21. The traction of $S_{max} = 0.1$ MPa implies essentially very weak bonding strength at the interfaces in the microstructures. The strength level of $S_{max} = 1000$ MPa, which is much higher than the intergranular bonding strength between HMX crystals ($S_{max}^{HMX} = 100$ MPa as in Ref. 5), is a hypothetical value used to explore trend in the ignition probability of microstructures with a very high interfacial strength level.

The second microstructure group has samples with interfacial bonding strengths that vary spatially. The stochastic variations of the maximum traction occur at the grain-binder interfaces, not inside the grains or the binder. The bonding strength is assumed to follow the Gaussian distribution with an average of 35 MPa, which is one of the six uniform values in the first group. The standard deviation of the bonding strength is 7 MPa, which is 20% of the average value, as shown in Fig. 4(a). The selection of the standard deviation follows the experimental results in Ref. 21, which show a scatter of 10–20% around a linear fit of data near the maximum cohesive stress. As an example of the spatially varying interfacial strength, Figs. 4(b) and 4(c) show a close up view of HMX grain boundaries, with the color coding of the strength levels given in Fig. 4(a). The constitutive relation of cohesive bonding is described in Ref. 31, and the values of the cohesive parameters for the first and second microstructure groups are listed in Table I. The material property parameters (i.e., elastic moduli and density) are listed in Table II (Ref. 32).

In the following discussion, "M_U" refers to the microstructure with uniform interfacial bonding strength, and "M_V" refers to the microstructure with stochastic variations in interfacial bonding strength.

B. Loading configuration

Figure 4(d) shows the loading configuration used. The sample size is 15 mm $\times$ 3 mm. A low impact velocity yields a distribution of ignition probability that is wider than a high impact velocity does for a statistically similar microstructure set, as reported in Ref. 7, accentuating the effect of the random morphological variations in the materials' microstructures. However, a low impact velocity lengthens the time to criticality, necessitating a larger microstructure for the simulation in order to avoid stress wave reflection from

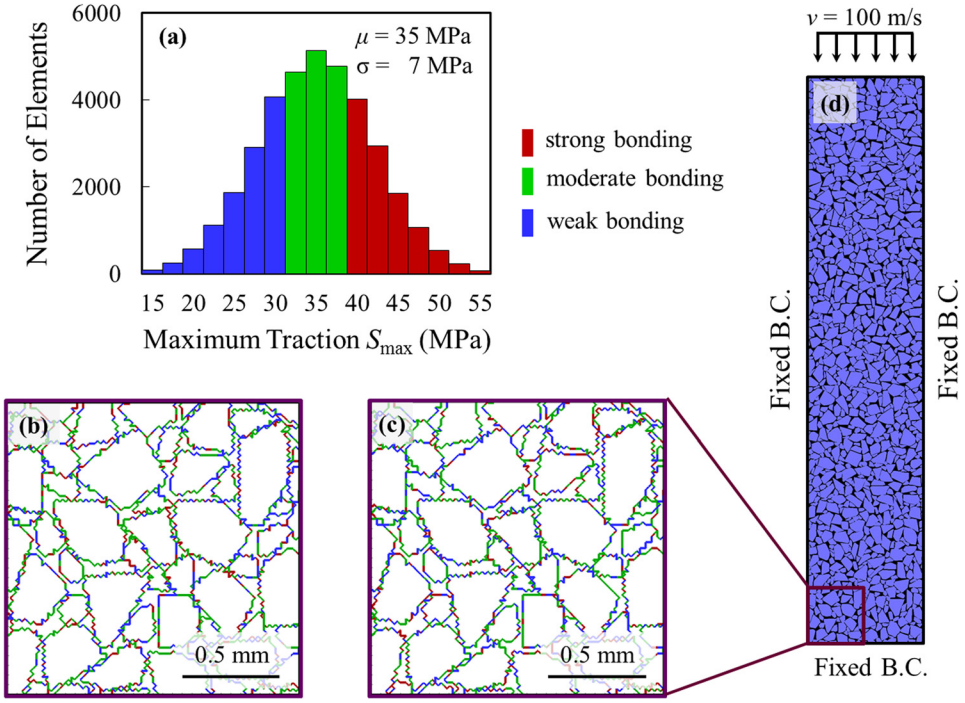

FIG. 4. Illustration of microstructures with spatially varying bonding strength between the HMX grains and Estane binder; (a) Gaussian distribution of the interfacial strength (mean (μ) = 35 MPa, standard deviation (σ) = 7 MPa); (b) and (c) Spatially varying interfacial bonding along boundaries between HMX grains and Estane binder, the red, green, and blue colors represent strong, moderate, and weak bonding strength levels, respectively; and (d) Configuration of the loading and boundary conditions used in the analysis.

the opposite fixed end of the sample. At an impact velocity of $v = 100$ m/s, approximately ~9.5 μs of loading and response without stress wave reflection can be analyzed.

The microstructure is initially stress-free and at rest. Once loading begins, the impact velocity is imposed at the top end of the sample shown in Fig. 4(d). Over the initial period of time ($0 \leq t < 0.5\,\mu$s), the boundary velocity is linearly ramped from zero to the maximum of $v = 100$ m/s. The left and right side boundaries are constrained such that lateral motions do not occur. This configuration approximates the normal impact loading of an infinitely wide material block under the conditions of macroscopically uniaxial strain. For all calculations presented, initial temperature is $T = 300$ K.

C. Ignition criterion

The ignition criterion provides a relationship between the size and the temperature of critical hotspots as

$$d(T) \geq d_c(T), \tag{1}$$

where d is the diameter of a hotspot resulting from a loading event whose interior temperatures are at or above temperature T and d_c is the minimal diameter of a hotspot required for thermal runaway at temperature T. The quantitative information regarding the right-hand side of Eq. (1) is taken from the work of Tarver *et al.*,[33] who performed chemical kinetics calculations to analyze the criticality issue for HMX and TATB explosives. The calculations consider multistep reaction mechanisms and the pressure and temperature dependence of reactants and products. [See Ref. 7 for details].

The left-hand side of Eq. (1) is obtained by analyzing the hotspot distributions from CFEM calculations. To account for the variations of temperature within a hotspot (note that temperatures at different spatial locations within a hotspot are different and the temperature threshold is the lowest temperature at the periphery), the criterion of Tarver *et al.* is defined by a band of ±10% about the mean value as in the previous publications. A hotspot is considered to be critical when it crosses the lower threshold limit (90% of the average threshold). Taking into consideration, the stochastic nature of arbitrary microstructures, we employ an approach to identify the time to criticality t_c measured from the onset of dynamic loading. Specifically, instead of one single hotspot, criticality is regarded as being reached if the critical hotspot density in a specimen reaches a level equal to or greater than 0.22 mm^{-2}. This level corresponds to two critical hotspots in a 3 mm square domain.

TABLE I. Cohesive parameters at grain-binder interface.

Types of bonding strength	Maximum traction S_{max} (MPa)
Random variation in strengths (Gaussian Distribution)	μ: 35 S_{max}: 7
Uniform strength	0.1 17.5 35 70 175

TABLE II. Material parameters for HMX and Estane.

Material Property	HMX	Estane
Bulk modulus K (MPa)	15700	3650
Shear modulus G (MPa)	8300	Prony series[32]
Density ρ (g/cm^3)	1.90	1.19

D. Issues analyzed

The analysis is performed in the following steps. First, calculations are carried out using multiple sets of instantiations described in Sec. II A with the loading condition shown in Fig. 4(d). Following the calculations, the ignition criterion described in Sec. II C is used to scan the microstructure for hotspots and detect critical hotspots that have reached the size-temperature threshold. With this approach, once an ensemble (or a set of microstructure instantiations) is defined, the distribution of the time to criticality can be uniquely determined for the microstructure set. For each set with a given combination of statistically similar attributes, the time to criticality (t_c) is evaluated as a cumulative probability distribution. The distribution of the time to criticality obtained from each set is fitted to the Weibull distribution with three parameters[34] in the form of

$$P(t) = 1 - e^{-\Phi(t)}, \quad \Phi(t) = \begin{cases} 0, & t \le t_0 \\ \left(\dfrac{t - t_0}{\tau}\right)^m, & t \ge t_0; \end{cases} \tag{2}$$

where t is the time to criticality, t_0 is the minimum time to criticality, or the cutoff time to criticality below which the probability of ignition is zero, τ is a time-scaling parameter that affects the slope of the distribution curve, and m is a shape parameter. From the Weibull equation, the median time to criticality (t_{50}) can be obtained by

$$t_{50} = t_0 + \tau[\ln(2)]^{1/m}. \tag{3}$$

Barua *et al.*[7] provided a physical basis for the Weibull distribution fit to the probability of time to criticality using Terao's model.[35] They showed that m= 2 for loading conditions involving a propagating stress wave front, which is the case for the configuration in Fig. 4(d) and throughout this paper. Under the condition that the shape parameter (m) has a constant value of 2, the Weibull distribution in Eq. (2) is determined by two parameters, one is the median time to criticality (t_{50}) and the other is the time-scaling parameter (τ). The relationship between parameters in Eq. (2) is given by Eq. (3).

The microstructure and CFEM model we utilize in this paper are two-dimensional, with conditions of plane strain. It is worth noting that the cutoff impact velocity obtained using this framework is in good agreement with the threshold velocity for ignition measured from experiments.[7] Although desirable, a three-dimensional framework would be much more computationally intensive and numerically challenging. Such a framework which needs to account for all the physical processes considered by the 2D framework here, including distributed fracture, internal friction, and frictional heating, is not currently available.

III. RESULTS AND DISCUSSION

A systematic quantification of the probabilistic distributions of time to criticality is carried out, focusing on (i) the effect of different levels of uniform interfacial strength $(S_{max} = 0.1 - 1000\,\text{MPa})$ (ii) the effect of random variations in the interfacial strength about the mean value, (iii) the effect of random phase morphology variations, and (iv) the combined effect of random interfacial bonding and microstructure morphological variations.

A. Probability of ignition with uniform interface strength

To provide a basis for systematic comparison, the probability of ignition for microstructures with spatially uniform interfacial bonding strength is analyzed. The analysis involves a microstructure group consisting of six sets of instantiations, as described in Sec. II A. Each set of instantiations has one of six uniform interfacial strength levels (S_{max} = 0.1, 17.5, 35, 70, 100, and 1000 MPa). The loading condition analyzed is that described in Fig. 4(d), and the ignition criterion used is that described in Sec. II C. In the following discussion, "Distribution-U" refers to the ignition probability distribution that results from random variations of phase morphology among statistically similar (see Ref. 7 for the definition and quantification) microstructures with uniform interfacial bonding strength (M_U). The Distribution-U's from the six sets of instantiations are shown in Fig. 5(a). The median time to criticality increases as the interfacial bonding strength increases (see Fig. 5(b)). The microstructures with very high interfacial strength (e.g., S_{max} = 1000 MPa) in general require longer times to reach criticality, such that many of them do not reach critical within the time window of loading without reflection from the bottom boundary (up to ~9.5 μs).

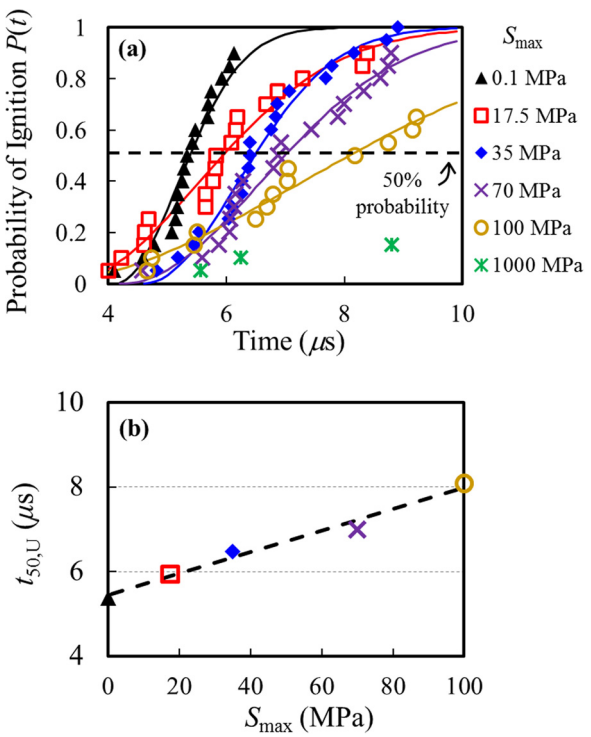

FIG. 5. Effect of the level of uniform interfacial strength on the time to criticality; (a) Distributions of ignition probability for statistically similar microstructures with six levels of uniform interfacial strengths (S_{max} = 0.1, 17.5, 35, 70, 100, and 1000 MPa); (b) Median time to criticality (t_{50}) as a function of uniform interfacial strength.

The data are fitted to the Weibull distribution in Sec. II D for five of the six levels of uniform interface strength (S_{max} = 0.1, 17.5, 35, 70, and 100 MPa). The median times to criticality ($t_{50,U}$) calculated using Eq. (3) are a function of the interfacial strength (S_{max}) .The median time increases as the interfacial strength increases. The trend can be well described by a linear relation as in Fig. 5(b).

Since the time to criticality is determined by localized heating in the sample, a correlation exists between the hotspot development and time to criticality $t_{C,U}$. Two parameters, hotspot number density (number of hotspots per unit volume of material, N_U) and hotspot area fraction (A_U), are quantified from the twenty samples with uniform interfacial strength (M_U) of $S_{max} = 35$ MPa, and are related to the ignition time of corresponding microstructure. The threshold of $T = 400$ K is used to cut off the temperature field and detect hotspots at $t = 6\,\mu$s after impact. The top 3 mm × 3mm portion of the domain is analyzed. Figure 6(a) shows that microstructures with a higher number density of hotspots require less time to criticality, and Figure 6(b) shows the same trend for the total area fraction of hotspots. Overall, more hotspot quantities (i.e., area fraction and number density of hotspots) are observed from microstructures that ignite earlier time than from those that ignite later time, indicating that the development of hotspots is one factor that determines the ignition sensitivity of the microstructure.

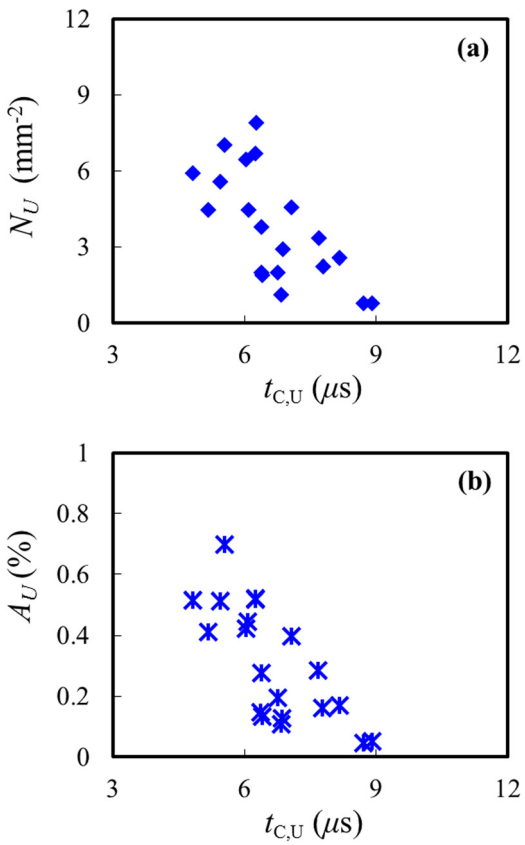

FIG. 6. Effect of hotspot field on the ignition time ($t_{C,U}$) of M_U; (a) Relation between the number density of hotspots (N_U) and $t_{C,U}$; (b) Relation between the total area fraction (A_U) of hotspots and $t_{C,U}$.

B. Effects of fluctuations in interface strength

The effect of spatial variations of the interface strength is analyzed using three microstructure samples. The first sample (M_U), which serves as a base line case for comparison, has uniform interface strength of $S_{max} = 35$ MPa. The other two samples (M_V) have the same microstructure morphology that the first sample has but involve stochastically varying interfacial strengths as described in Sec II A. Since the variations in interfacial strength are randomly distributed, the grain-binder configuration denoted by strength color of one microstructure among the two samples differs from that of the other microstructure as shown in Figs. 1(c) and 1(d). Figures 7(a)–7(c) show the temperature distributions for the three cases at 6 μs after impact. The overall appearances of the hotspot fields for the three bear resemblance. However, both locations and peak temperatures of the critical hotspots are different. The variations in interfacial bonding strength provide a perturbation to the thermomechanical processes in the materials, causing the temperature distributions to be different. For a microstructure set with the same phase morphology having random variations in interfacial strength, the stochastic growth of hotspot leads to the ignition time to be different from sample to sample, giving rise to the probability distribution of time to criticality.

The resemblance of hotspot field between M_U and M_V is quantified for all twenty microstructure morphologies. Specifically, twenty sets of new samples are generated, with each set based on a baseline microstructure morphology from one of the twenty microstructures of M_U, providing a total of 20 × 20 = 400 samples. All four hundred samples have randomly varying binder-grain bonding strengths as illustrated in Sec. II A. The number density and the total area of hotpots are obtained from each sample set of M_V. The average values of hotspot number density (N_V) and hotspot area fraction (A_V) from each sample set of M_V are related to the hotspot number density (N_U) and hotspot area fraction (A_V) from the baseline sample in M_U as shown in Figs. 8(a) and 8(b). The results show that the data points follow $N_V = N_U$ and $A_V = A_U$ closely, with a slight bias toward the side of the case with both sources of stochasticity, suggesting that the hotspot field is primarily determined by its microstructure morphology, and the variations in interfacial bonding strength makes perturbation on hotspot evolution.

C. Combined effects of variations in microstructural morphology and interface strength

The combined effect of two sources of stochasticity—phase morphology changes and variations in interfacial strength are analyzed. Among the twenty microstructures with the uniform interfacial strength of 35 MPa in the sample set described in Sec. III A, three microstructures are chosen as examples for this analysis. When they are assigned uniform interfacial strength, their ranking order of ignition times is as follows. The first microstructure, referred to as {A}, yields the earliest time to criticality ($t_{C,U}\{A\} = 4.82\,\mu$s); the second microstructure, referred to as {B}, yields the median time to criticality ($t_{C,U}\{B\} = 6.41\,\mu$s) among the twenty samples in the set; and the third microstructure chosen,

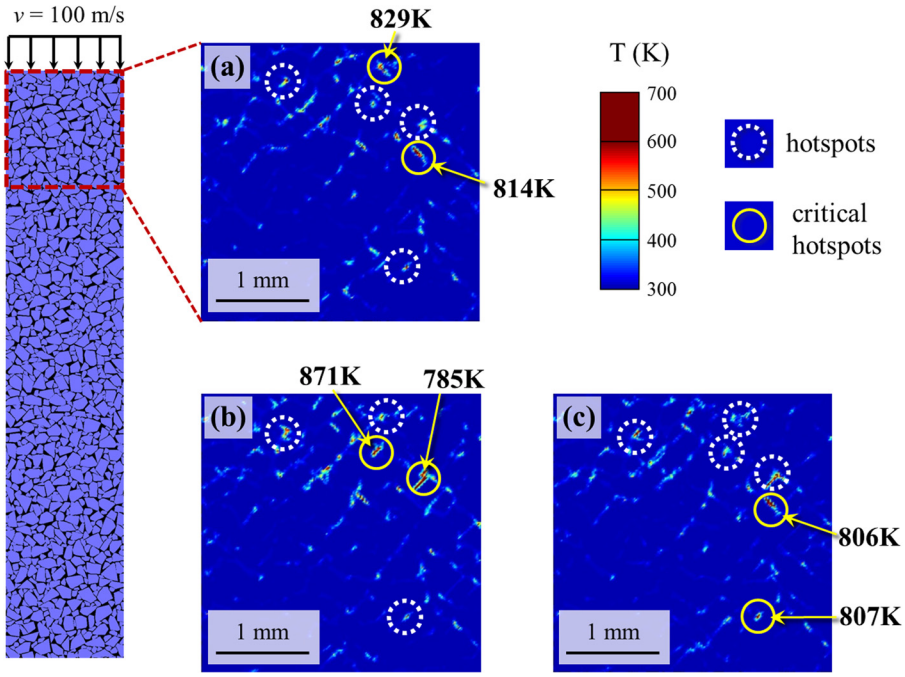

FIG. 7. Temperature field and hotspot locations at $t = 6\,\mu$s (a) from a microstructure with uniform interfacial strength and (b) and (c) from the same microstructure with varying interfacial strength. Circles indicate the hotspots (in white dotted line) and the critical hotspots (in yellow solid line).

referred to as {C}, yields the longest time to criticality ($t_{C,U}\{C\} = 8.92\,\mu$s) among the twenty samples as shown in Fig. 9(a). Now, these three samples are used to generate three new sets of samples, each based on one of the three original samples. These three new sets, each consisting of twenty samples, constitute a total of 60 samples. The samples in each set have the same microstructure morphology as the corresponding one among the three representative microstructures chosen (A, B, or C), but have binder-grain bonding strengths that vary randomly from location to location around the original uniform strength of 35 MPa (see Figs. 4(b) and 4(c)).

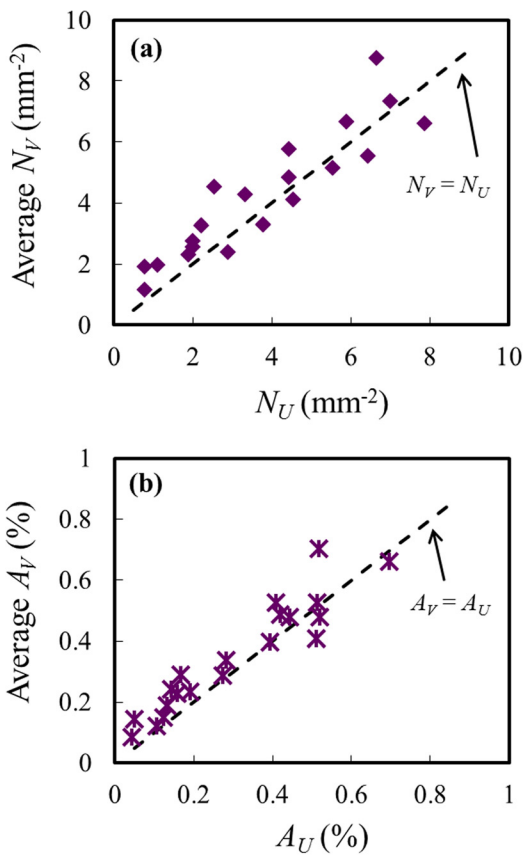

FIG. 8. Correlation between the hotspot field of M_U and the average quantity of hotspot field of M_V; (a) Relation between the average number density of hotspots (N_V) from M_V and the number density of hotspots (N_U) from M_U; (b) Relation between the average area fraction of hotspots (A_V) from M_V and the area fraction of hotspots (A_U) from M_U.

Figure 9(b) shows the probability of ignition as a function of time for the three new sets of microstructures. The term "Distribution-V" refers to the probability distribution of the time to criticality arising from the random fluctuations in interfacial strength only. In other words, each of the three new sets of samples yields one "Distribution-V". The results show that the Distribution-V's from the first microstructure (i.e., A), the second microstructure (i.e., B), and the third microstructure (i.e., C) lie between $4.42 - 6.23\,\mu$s, $5.19 - 8.41\,\mu$s, and $5.52 - 9.29\,\mu$s, respectively.

Two interesting features are observed when the Distribution-V's are compared with their baseline ignition times $t_{C,U}\{A\}$, $t_{C,U}\{B\}$, and $t_{C,U}\{C\}$) in Distribution-U. The first feature is that the baseline ignition time ($t_{C,U}\{A\}$, $t_{C,U}\{B\}$, or $t_{C,U}\{C\}$) in Distribution-U (Fig. 9(a)) is not the mean ignition time for the corresponding sample sets giving rise to Distribution-V. Specifically, for microstructure morphology {A} which has the shortest ignition time $t_{C,U}\{A\}$, the corresponding ignition times in Distribution-V are mostly later than $t_{C,U}\{A\}$ [note the dotted vertical line in Fig. 9(b)]. On the other hand, the opposite is observed for microstructure morphology {C} which has the longest ignition time $t_{C,U}\{C\}$—the corresponding ignition times in Distribution-V are mostly earlier. For microstructure morphology {B}, the corresponding ignition times in Distribution-V straddle both sides of $t_{C,U}\{B\}$.

The second feature is that the ranking order of mean ignition time of Distribution-V's for the three new sample

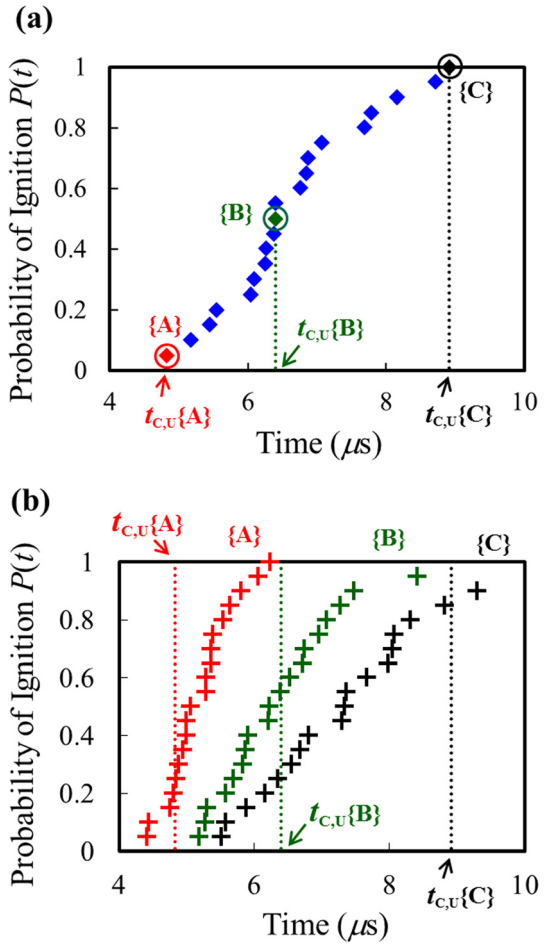

FIG. 9. Relation between Distribution-V and the ignition time of the corresponding M_U; (a) Distribution-U. The names {A}, {B}, and {C} represent the microstructure morphologies that generate the earliest ($t_{C,U}\{A\}$), median ($t_{C,U}\{B\}$), and latest ($t_{C,U}\{C\}$) time to criticality, respectively; (b) Distribution-V's from the selected microstructure morphologies, {A}, {B}, and {C}. The dotted vertical lines represent the ignition times of corresponding M_U in Fig. 9(a).

sets follow the same order of the ignition time for the three baseline microstructures in Distribution-U, i.e., $t_{C,U}\{A\}$, $t_{C,U}\{B\}$, and $t_{C,U}\{C\}$. As discussed in Sec. III B, the hotspot locations in the microstructures with uniform interfacial strength are similar to the hotspot locations in the corresponding microstructures with random fluctuations in interfacial strength around the uniform strength value, as seen in Figs. 7(a)–7(c). The similarity in hotspot locations shows that sites for the occurrence of dominant hotspots are primarily determined by microstructure morphology and material heterogeneity. In contrast, fluctuations in interfacial strength cause stochastic field (e.g., temperature) perturbations that "modulate" the degree of localization of the field quantities. As a result, variations in interfacial strength cause stochastic variations in ignition time relative to the ignition time determined by the material heterogeneity inherent in the microstructures.

Although only the results for three samples (A, B, and C) out of the twenty samples in Distribution-U are shown above, results for all twenty microstructures show the same features and trends. A total of 400 samples generated in Sec. III B are used, involving randomly varying binder-grain bonding strengths as illustrated in Sec. II A. The trend shown in Fig. 9 is analyzed for all twenty sets. To obtain an analytical quantification of the trend, both Distribution-U and Distribution-V are characterized using Weibull distribution functions. The specific forms used here are

$$P_1(t) = 1 - \exp\left[-\left(\frac{t - t_{0,U}}{\tau_U}\right)^2\right], \text{ and} \tag{4a}$$

$$P_2(t) = 1 - \exp\left[-\left(\frac{t - t_{0,V}}{\tau_V}\right)^2\right]. \tag{4b}$$

Here, subscript "U" denotes the value obtained from Distribution-U, and subscript "V" denotes the value obtained from Distribution-V.

The dependency of Distribution-V on Distribution-U is analyzed using the median time to criticality ($t_{50,V}$) and the time-scale parameter (τ_V) to capture the overall shift of the distribution with respect to time and the slope of the distribution. Subsequently, Eq. (3) is used to obtain the parameters in Eqs. (4a) and (4b). The median time to criticality ($t_{50,V}$) and time-scale parameter (τ_V) for Distribution-V for each sample set are related to, and therefore change with, the ignition time $t_{C,U}$ of the corresponding baseline microstructure

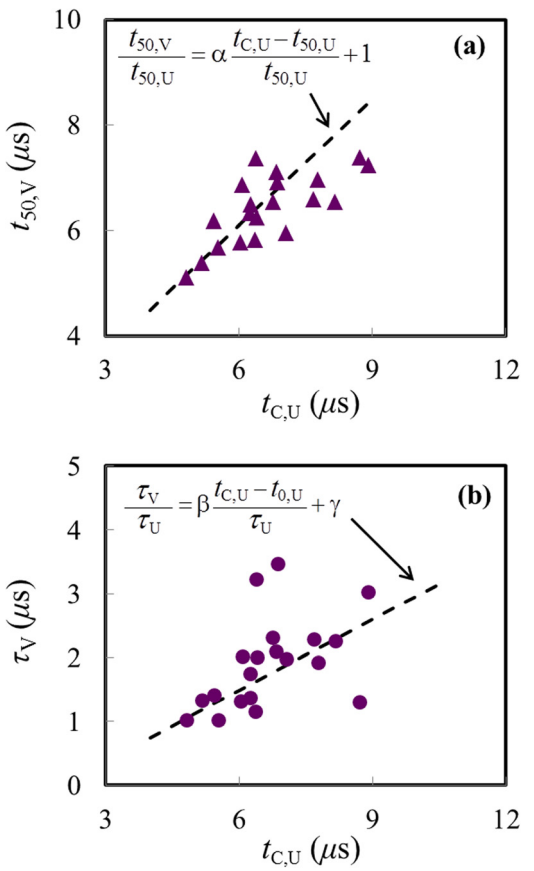

FIG. 10. Relation between the Weibull parameters of Distribution-V and the ignition time of M_U ($t_{C,V}$) with the corresponding morphology; (a) Relation between the minimum time to ignition ($t_{0,V}$) for Distribution-V and $t_{C,U}$ in Distribution-U; (b) Relation between the median time to ignition ($t_{50,V}$) for Distribution-V and $t_{C,U}$ in Distribution-U.

TABLE III. Parameters used in Eqs. (5a) and (5b).

Parameters	Values (dimensionless)
α	0.8
β	1
δ	0.37
γ	0.43

in Distribution-U as shown in Figs. 10(a) and 10(b). The relations are represented by

$$\frac{t_{50,V}}{t_{50,U}} = \alpha\left(\frac{t_{C,U} - t_{50,U}}{t_{50,U}}\right) + \beta, \text{ and} \tag{5a}$$

$$\frac{\tau_V}{\tau_U} = \gamma\left(\frac{t_{C,U} - t_{0,U}}{\tau_U}\right) + \delta, \tag{5b}$$

where the parameters α, β, γ, and δ are fitting constants. The values of those constants are listed in Table III.

Parameter α represents the strength of the effect of morphology variations on the median time to criticality of Distribution-V. A value of $\alpha = 1$ would indicate a simple direct superposition of the morphology variation effect and the property fluctuation effect for the mean ignition time for Distribution-V. A value of $\alpha = 0$ would mean no morphology variation effect on the mean ignition time for Distribution-V. Values of α that are between 1 and 0 indicate the second source of stochasticity "diminishes" the effect of the first source of stochasticity. For the conditions studied, the value of $\alpha = 0.8$ suggests that the influence of the first source is more dominant than that of the second source on the median time to criticality $(t_{50,V})$ of Distribution-V.

Parameter β represents the potential scaling of the mean ignition time for Distribution-U that may be required in order to arrive at the ignition times for samples in Distribution-V due to the introduction of the second source of stochasticity (the random fluctuations in interfacial strength). A value of $\beta = 1$ indicates no scaling here. Parameters γ and δ quantify the ratio between the slope of Distribution-V and the slope of Distribution-U. Parameter γ embodies the dependency of the ignition probability distribution associated with Distribution-V on the first source of stochasticity. A value of $\gamma = 0$ would indicate that the slopes of all Distribution-V curves are the same. Higher γ values would suggest stronger dependence of Distribution V probability profiles on Distribution-U. The value obtained for the conditions studied is $\gamma = 0.43$. Parameter δ alone determines the slope of the Distribution-V ignition probability curve for the sample with the microstructure morphology that generates the minimum time to criticality (ideally most ignition sensitive microstructure morphology in Distribution-U) as a function of the slope of the ignition time probability profile associated with Distribution U.

Since all 400 samples have statistically similar microstructure morphologies and the same average interfacial strength with the same level of stochastic variations, their times to criticality can also be treated as one statistical ensemble. Such an analysis is carried out in Fig. 11. The result

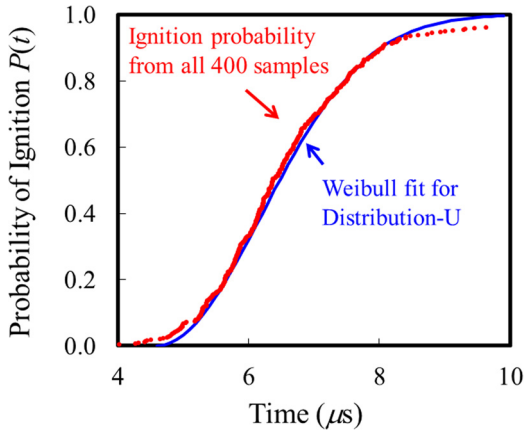

FIG. 11. Distribution of ignition probability from all 400 samples (red line) in comparison with the Weibull fit for Distribution-U (blue line).

provides an overall quantification of the ignition behavior of the samples with two sources of stochasticity. The result also raises the question of "how do the contributions of the two sources combine to yield the overall behavior in Fig. 11?".

D. Combined models

The first step in developing a model to quantify the combined probability of ignition accounting for both sources of stochasticity is to quantify the probability distributions due to each source, as this quantification provides the basis for superposition. The behaviors of both Distribution-U and Distribution-V are described by the Weibull distribution functions as in Eqs. (4a) and (4b).

To analyze the combined effect of the two types of stochastic variations, two models based on these individual quantifications are first examined. These models are simple parallel and series arrangements shown in Figs. 12(a) and 12(b). The idea of parallel and serial arrangements, as discussed in Ref. 36, was originally developed to consider the failure of mechanical systems consisting of many components. The failure of one component of a system is independent of the failure of other components. In the parallel model, the system fails when all components fail. In the serial model, the system fails if any of its components fails.

The superimposed probabilities of ignition for parallel and serial systems are given by [see Ref. 36 for derivations]

$$P_{para}(t) = \left[1 - \exp\left\{-\left(\frac{t - t_{0,U}}{\tau_U}\right)^2\right\}\right] \times \left[1 - \exp\left\{-\left(\frac{t - t_{0,V}}{\tau_V}\right)^2\right\}\right], \tag{6a}$$

$$P_{serial}(t) = 1 - \exp\left\{-\left(\frac{t - t_{0,U}}{\tau_U}\right)^2 - \left(\frac{t - t_{0,V}}{\tau_V}\right)^2\right\}. \tag{6b}$$

As discussed in Ref. 36, a parallel system becomes more likely to survive as components are added it, because the probability of failure of the system is obtained by multiplying the failure probabilities of all components. On the other

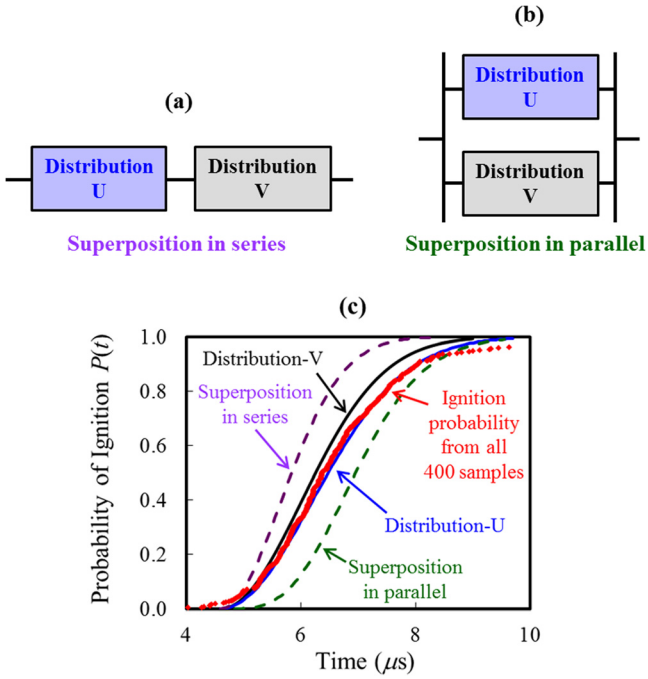

FIG. 12. Schematics for (a) series and (b) parallel systems,[36] and (c) combined probability in series (violet line) and in parallel (green line) system of Distribution-U (blue line) and Distribution-V (black line) from a microstructure that has the ignition time of $t_c = 6.4\ \mu s$.

hand, a serial system becomes more likely to fail as more components are added, because the survivability of a system is obtained by multiplying the survivabilities of all components.

Figure 12(c) shows Distribution-U (blue), Distribution-V (black), along with the combined probabilities in series (purple) and in parallel (green). Combining the individual probabilities in a serial fashion shifts the combined probability toward earlier times. On the other hand, combining the individual probabilities in a parallel fashion shifts the combined probability toward later times. Both are far from what is observed in Fig. 11 which shows that the combined probability distribution of ignition does not shift in either earlier or later time directions relative to the Distribution-U curve. The actual combined probability curve is simply more spread out toward both early time and long time extremes. Note that the parallel and serial models assume that the probability of a component's failure is independent of that of other components in the same system.[36] Here, the parameters for Distribution-V may depend on Distribution-U. These factors and the differences in Fig. 12 point out the need for a new mathematical model for combining the two probability functions in Eqs. (4a) and (4b).

E. Nested probability distribution model

To arrive at the joint probability distribution, we propose a nested probability superposition model that combines the effects of the two sources of stochasticity on ignition probability. This nested probability model recognizes the fact that there are "two layers" of probability distributions. The first layer is due to random variations in microstructure morphology. The second layer is associated with the fluctuations in interfacial bonding strength. Note that the random fluctuations in bonding strength can only occur along the boundaries between the binder and the energetic granules, and the discussion of fluctuations in bonding can only be pursued for given microstructures. Because of this constraint, the variations in microstructure morphology must be treated as the first layer of variations which can be made regardless of interfacial strength. On the other hand, the fluctuation in bonding is a second level variation that "rides" with the microstructure, and therefore, is treated as the secondary variation here. This "layering" of variations determines the order or manner in which the superposition of the two levels of probability distributions is carried out. The nested superposition model developed here reflects this fact.

El Otmani *et al.*[37] considered a nested probability of the Gaussian distribution. For the first layer, there are n number of random values that follow the Gaussian distribution (μ, σ_1^2), where μ is the mean and σ_1 is the standard deviation. An arbitrary point among the n values $(x_1, \ldots, x_n)$ is denoted as x_i. For the second layer, there are n sets of values, and the values in each set follow a new Gaussian distribution with the mean value of x_i (from the first layer) and a standard deviation of σ_2. If the values from all sets are combined, then the probability density function[37] that represents the population of all values is

$$f(x) = \frac{1}{\sqrt{2\pi(\sigma_1^2 + \sigma_2^2)}} \exp\left\{-(x-\mu)^2 / \left[2(\sigma_1^2 + \sigma_2^2)\right]\right\}. \quad (7)$$

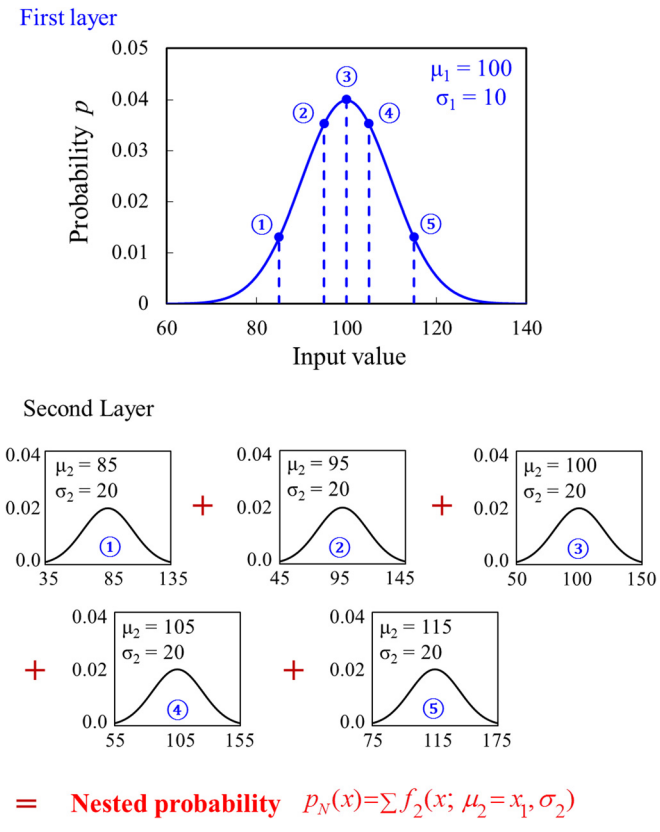

FIG. 13. Conceptual diagram for the nested probability function of Gaussian distribution.

Figure 13 shows a conceptual illustration of the nested probability function of the Gaussian distribution.

To analyze the how effects of the two sources of variations (in morphology and interfacial strength) combine, we consider a large number of random values that follow the nested probability model. For the first layer, 100 000 random values that follow the Weibull function of Distribution-U [Eq. (4a)] are generated. For the second layer, the same number of sets of random values are generated based on the values in the first layer. The random values of each set in the second layer follow the Weibull function of Distribution-V [Eq. (4b)]. The Weibull parameters $t_{0,V}$ and τ_V in Eq. (4b) are obtained using the linear relation between $t_{C,U}$ and τ_V and the linear relation between $t_{C,U}$ and $t_{50,V}$ as discussed in Sec. III C.

Ultimately, the properly superimposed, combined ignition probability function must agree with the total ignition probability function obtained with all cases which are considered as a statistical ensemble of one sample set. Figure 14 shows the combined distribution function obtained by using the nested probability (green dots) and the probability distribution of time to criticality represented by all 400 samples (red line). The closeness between the two curves confirms the validity of the nested superposition model and the insights it yields.

In order to obtain an analytical form of the nested Weibull probability distribution, a finite, discrete mixture model is considered. A general form for this model[38] is

$$P(t) = \sum_{i=1}^{n} w_i p_i(t), \tag{8}$$

where $w_i \geq 0$ are weighs for the individual probability density functions $p_i(t)$ for each set of samples in the second layer. The parameters in Eq. (8) that represent the combined probability are $w_i = 1/n$, $n = 20$. The probability $p_i(t)$ is stated in the form of

$$p_i(t) = H(t - t_{0,i}) \frac{2}{\tau_i} \left(\frac{t - t_{0,i}}{\tau_i} \right) \cdot \exp\left\{ -\left(\frac{t - t_{0,i}}{\tau_i} \right)^2 \right\}, \tag{9}$$

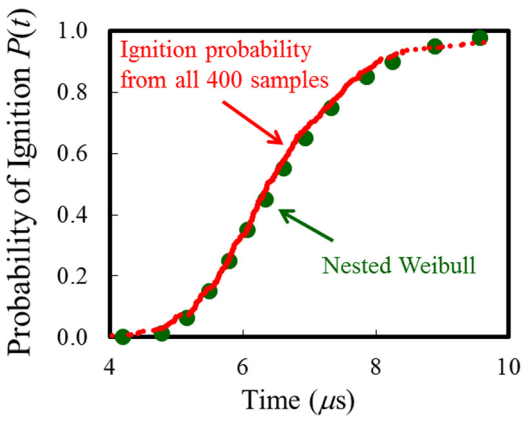

FIG. 14. The nested Weibull distribution obtained by generating large number of random values (greed dots) and the probability distribution data from all 400 instantiations (red line).

where $H(\bullet)$ is the Heaviside unit step function, and $t_{0,i}$ and τ_i are $t_{0,V}$ and τ_V for the i-th microstructural morphology, respectively. The finite, discrete mixture of Weibull distribution functions is equivalent to the nested Weibull distribution, representing the combined probability of ignition. However, the finite mixture of probability distributions is a summation of discrete probability functions. A concise analytical form of the final probability as a continuous function has not yet been obtained through this approach.

In Eq. (9), the probability function $p_i(t)$ can be represented as a conditional probability, $p_i(t|t_c)$, because $p_i(t)$ is valid only if the microstructure with the corresponding morphology ignited at $t = t_{C,U}$. The probability of ignition for an arbitrary sample among a statistical ensemble of all samples is mathematically known as the *joint probability*, $p(t, t_c)$ of two probability functions—a conditional probability function of Distribution-V and a probability function for Distribution-U. That is,

$$\begin{aligned} p(t, t_c) &= p(t|t_c) \cdot p(t_c) \\ &= H(t - t_{0,i}) \cdot \frac{2}{\tau_i} \left(\frac{t - t_{0,i}}{\tau_i} \right) \cdot \exp\left\{ -\left(\frac{t - t_{0,i}}{\tau_i} \right)^2 \right\} \\ &\quad \times H(t_{C,U} - t_{0,U}) \cdot \frac{2}{\tau_U} \left(\frac{t_{C,U} - t_{0,U}}{\tau_U} \right) \\ &\quad \times \exp\left\{ -\left(\frac{t_{C,U} - t_{0,U}}{\tau_U} \right)^2 \right\}. \end{aligned} \tag{10}$$

If all possible microstructures are considered, the final combined probability density function (PDF) is

$$\begin{aligned} p(t) = \int_{t_{C,U}=t_{0,mor}}^{\infty} & \left[H(t - t_{0,i}) \cdot \frac{2}{\tau_i} \left(\frac{t - t_{0,i}}{\tau_i} \right) \right. \\ & \times \exp\left\{ -\left(\frac{t - t_{0,i}}{\tau_i} \right)^2 \right\} \cdot \frac{2}{\tau_U} \left(\frac{t_{C,U} - t_{0,U}}{\tau_U} \right) \\ & \left. \times \exp\left\{ -\left(\frac{t_{C,U} - t_{0,U}}{\tau_U} \right)^2 \right\} \right] dt_{C,U}, \end{aligned} \tag{11}$$

and the cumulative distribution function (CDF) is

$$\begin{aligned} P(t) = \int_{\xi=0}^{t} f(\xi) \cdot d\xi = \int_{\xi=0}^{t} \int_{t_{C,U}=t_{0,V}}^{\infty} & \left[H(\xi - t_{0,i}) \cdot \frac{2}{\tau_i} \left(\frac{\xi - t_{0,i}}{\tau_i} \right) \cdot \exp\left\{ -\left(\frac{\xi - t_{0,i}}{\tau_i} \right)^2 \right\} \right. \\ & \left. \times \frac{2}{\tau_U} \left(\frac{t_{C,U} - t_{0,U}}{\tau_U} \right) \cdot \exp\left\{ -\left(\frac{t_{C,U} - t_{0,U}}{\tau_U} \right)^2 \right\} \right] dt_{C,U} \cdot d\xi, \end{aligned} \tag{12}$$

where τ_i and $t_{0,i}$ are $t_{0,V}$ and τ_V as obtained from Eqs. (3), (5a), and (5b).

Figure 15 shows the CDF obtained from a numerical integration of Eq. (12) [shown in black line], and the nested Weibull function [shown in green dots]. The distributions

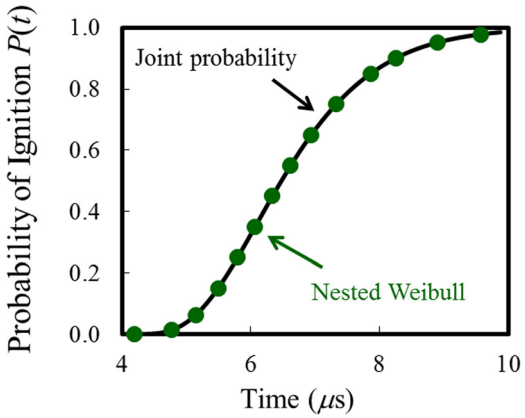

FIG. 15. The nested Weibull distribution (green dots) and the CDF from the equation of the Joint probability function (black line).

from the two approaches provide identical results, confirming that Eqs. (11) and (12) are the analytical forms of the nested Weibull distribution.

It should be pointed out that, in the nested probability model, we first obtained the relations between the parameters for distributions associated with the variations in morphology and interfacial strength. Subsequently, we used these relations to obtain the analytical form of the final probability. In experiments, however, the approach is often reversed, and it is not straightforward to separate the effect of one source of variations from the effect of another. For example, Subero-Couroyer *et al.*[39] performed experiments on the crushing probability of particles with multiple sources of defects. The crushing probabilities arising from each source of defects and multiple sources of defects are quantified using Weibull distribution functions. The Weibull function for samples with multiple sources of coupled defects is equivalent to the nested Weibull function in our model. However, as indicated in Ref. 39, "it is difficult to separate the effect of macroporosity from the combined effect of macroporosity and defects…". The reversed approach to isolate or separate the effects from the nested Weibull function can be the topic of a future study.

IV. CONCLUSION

This study focuses on the effects of multiple sources of material stochasticity on the probability of ignition of PBXs under impact loading. The analysis carried out in this paper concerns two types of variations. The first is in microstructural morphology, and the second is in grain-binder interfacial bonding strength. Each source of variations gives rise to a degree of randomness in the locations, sizes and temperatures of hotspots which in turn results in a degree of randomness in the ignition behavior of the materials.

Two sets of calculations are performed. The first set focuses on the effect of the microstructures that have random variations in morphology, but different levels of spatially uniform bonding strength. The result shows a linear relationship between interfacial strength and median time to criticality of ignition probability. For a given level of uniform bonding strength $(e.g., S_{\max} = 35\,\text{MPa})$, microstructures with more intense hotspots (i.e., higher area fraction and number density of hotspots above a certain threshold) result in earlier ignition than those with less intense hotspots. The second set utilizes the microstructures with random variations in morphology from the first set and adds random fluctuations in interfacial strength to each sample. The result shows that the hotspot attributes—locations, number density, and area fractions—from the microstructures in the second set bear strong resemblance to the hotspot features from the microstructure with the morphology and uniform bonding strength. This resemblance is the underlying reason why the ignition probability distribution due to fluctuations in interfacial strength is dependent on the ignition time of the baseline microstructure morphology.

To understand how the different sources combine to affect the overall ignition behavior, we developed a nested superposition model. The results show that the model captures the interactions between the two sources of variations in material attributes. Although only two sources of stochasticity are considered here, the model can be generalized to analyze the combined effects of multiple sources of stochasticity. It must be pointed out that, in experiments, the final data set comes out as combined probability in most cases, and separation of the effects of the individual sources is often challenging. This separation is only studied here using the two-layered models and simulations. A separation without such systematic sets of calculations has not been attempted. Developing an inverse approach that starts with the final combined data to obtain the effects of individual sources and the relations between the effects of individual sources of heterogeneities can be a useful endeavor in the understanding of the stochastic behavior of heterogeneous materials.

ACKNOWLEDGMENTS

The authors gratefully acknowledge support from the Defense Threat Reduction Agency (DTRA) and Air Force Research Laboratory (AFRL) at the Eglin AFB (DISTRIBUTION A, approved for public release, distribution unlimited, 96ABW-2014-0042). Calculations are carried out on parallel computers at DPRL at Georgia Tech.

[1]M. H. Keshavarz and H. R. Pouretedal, "Simple empirical method for prediction of impact sensitivity of selected class of explosives," J. Hazard. Mater. **124**, 27–33 (2005).
[2]B. W. Asay, *Non-Shock Initiation of Explosives* (Springer, 2010).
[3]A. Barua, Y. Horie, and M. Zhou, "Energy localization in HMX-Estane polymer-bonded explosives during impact loading," J. Appl. Phys. **111**, 054902 (2012).
[4]A. Barua, Y. Horie, and M. Zhou, "Microstructural level response of HMX-Estane polymer-bonded explosive under effects of transient stress waves," Proc. Roy. Soc. A-Math. Phys. Eng. Sci. **468**, 3725–3744 (2012).
[5]A. Barua and M. Zhou, "A Lagrangian framework for analyzing microstructural level response of polymer-bonded explosives," Model. Simul. Mater. Sci. Eng. **19**, 055001 (2011).
[6]A. Barua, S. Kim, Y. Horie, and M. Zhou, "Ignition criterion for heterogeneous energetic materials based on hotspot size-temperature threshold," J. Appl. Phys. **113**, 064906 (2013).
[7]A. Barua, S. Kim, Y. Horie, and M. Zhou, "Prediction of probabilistic ignition behavior of polymer-bonded explosives from microstructural stochasticity," J. Appl. Phys. **113**, 184907–184920 (2013).
[8]J. E. Field, N. K. Bourne, S. J. P. Palmer, S. M. Walley, J. Sharma, and B. C. Beard, "Hot-spot ignition mechanisms for explosives and propellants [and Discussion]," Philos. Trans. Phys. Sci. Eng. **339**, 269–283 (1992).

[9]J. Dienes and J. Kershner, *Multiple-Shock Initiation Via Statistical Crack Mechanics*, Los Alamos National Lab., NM (United States) 1998.
[10]J. K. Dienes, J. Middleditch, J. D. Kershner, Q. Zuo, and A. Starobin, "Progress in statistical crack mechanics: An approach to initiation," in *Proceedings of the 12th Symposium (International) on Detonation* (2002).
[11]J. K. Dienes, Q. H. Zuo, and J. D. Kershner, "Impact initiation of explosives and propellants via statistical crack mechanics," J. Mech. Phys. Solids **54**, 1237–1275 (2006).
[12]A. L. Nichols III and C. M. Tarver, "A statistical hot spot reactive flow model for shock initiation and detonation of solid high explosives," in *Twelfth International Symposium on Detonation, Office of Naval Research, San Diego, CA* (2002).
[13]Y. Hamate and Y. Horie, "A Statistical Approach on Mechanistic Modeling of High-Explosive Ignition," AIP Conf. Proc. **706**, 335–338 (2004).
[14]G. N. Hassold and D. J. Srolovitz, "Brittle-fracture in materials with random defects," Phys. Rev. B **39**, 9273–9281 (1989).
[15]P. M. Duxbury, S. G. Kim, and P. L. Leath, "Size effect and statistics of fracture in random materials," Mater. Sci. Eng. A **176**, 25–31 (1994).
[16]J. Andersons, E. Porikže, and E. Spārniņš, "The effect of mechanical defects on the strength distribution of elementary flax fibres," Compos. Sci. Technol. **69**, 2152–2157 (2009).
[17]V. V. Silberschmidt and J. L. Chaboche, "The effect of material stochasticity on crack damage interaction and crack-propagation," Eng. Fract. Mech. **48**, 379–387 (1994).
[18]W. Yan-Qing and H. Feng-Lei, "A micromechanical model for predicting combined damage of particles and interface debonding in PBX explosives," Mech. Mater. **41**, 27–47 (2009).
[19]J. N. Plohr, B. E. Clements, and F. L. Addessio, "Dynamically driven phase transformations in damaged composite materials," in *Shock Compression of Condens Matter - 2005, Pts 1 and 2,* vol. 845, pp. 266–269, 2006.
[20]H. Tan, Y. Huang, C. Liu, G. Ravichandran, and G. H. Paulino, "Constitutive behaviors of composites with interface debonding: The extended Mori-Tanaka method for uniaxial tension," Int. J. Fract. **146**, 139–148 (2007).
[21]H. Tan, C. Liu, Y. Huang, and P. H. Geubelle, "The cohesive law for the particle/matrix interfaces in high explosives," J. Mech. Phys. Solids **53**, 1892–1917 (2005).
[22]K. Yanase and J. W. Ju, "Effective elastic moduli of spherical particle reinforced composites containing Imperfect interfaces," Int. J. Damage Mech. **21**, 97–127 (2012).
[23]M. Ostoja-Starzewski, P. Y. Sheng, and I. Jasiuk, "Influence of random geometry on effective properties and damage formation in composite materials," J. Eng. Mater. Technol. **116**, 384–391 (1994).
[24]S. S. Vel and A. J. Goupee, "Multiscale thermoelastic analysis of random heterogeneous materials Part I: Microstructure characterization and homogenization of material properties," Comput. Mater. Sci. **48**, 22–38 (2010).
[25]A. J. Goupee and S. S. Vel, "Multiscale thermoelastic analysis of random heterogeneous materials Part II: Direct micromechanical failure analysis and multiscale simulations," Comput. Mater. Sci. **48**, 39–53 (2010).
[26]A. M. Freudenthal, "Statistical approach to brittle fracture," in *Fracture: An Advanced Treaties*, edited by H. Liebowitz, Vol. 2 (Academic Press, New York and London, 1971).
[27]S. Chakravarthy, K. A. Gonthier, and R. Panchadhara, "Analysis of mesoscale heating by piston supported waves in granular metalized explosive," Modell. Simul. Mater. Sci. Eng. **21**, 055016 (2013).
[28]R. Menikoff, "Compaction wave profiles in granular HMX," in *Shock Compression of Condensed Matter-2001, Pts 1 and 2, Proceedings*, edited by M. D. Furnish *et al*., Vol. 620 (Amer Inst Physics, Melville, 2002), pp. 979–982.
[29]C. Liu, "Specific surface: A missing parameter in high-explosive modeling," Los Alamos National Laboratory (LANL), Los Alamos, NM (United States), Report No. LA-UR-14-20512, 2003.
[30]E. M. Mas, B. E. Clements, A. Ionita, and P. Peterson, "Finite element method calculations on statistically consistent microstructures of PBX 9501," AIP Conf. Proc **845**, 487–490 (2006).
[31]J. Zhai, V. Tomar, and M. Zhou, "Micromechanical simulation of dynamic fracture using the cohesive finite element method," J. Eng. Mater. Technol. **126**, 179–191 (2004).
[32]E. M. Mas, B. E. Clements, W. R. Blumenthal, C. M. Cady, G. T. Gray, and C. Liu, "A viscoelastic model for PBX binders," in *Shock Compression of Condensed Matter-2001, Pts 1 and 2, Proceedings*, Vol. 620, pp. 661–664, 2002.
[33]C. M. Tarver, S. K. Chidester, and A. L. Nichols, "Critical conditions for impact- and shock-induced hot spots in solid explosives," J. Phys. Chem. **100**, 5794–5799 (1996).
[34]Y. Li and M. Zhou, "Prediction of fracture toughness of ceramic composites as function of microstructure: I. Numerical simulations," J. Mech. Phys. Solids **61**, 472–488 (2013).
[35]K. Terao, *Irreversible Phenomena* (Springer, 2007).
[36]J. I. McCool, *Using the Weibull Distribution* (John Wiley & Sons, Inc., 2012).
[37]S. El Otmani and A. Maul, "Probability distributions arising from nested Gaussians," Comp. R. Math. **347**, pp. 201–204 (2009).
[38]G. K. Miller, *Probability: Modeling and Applications to Random Processes*, 1 ed. (Wiley, 2006).
[39]C. Subero-Couroyer, M. Ghadiri, N. Brunard, and F. Kolenda, "Weibull analysis of quasi-static crushing strength of catalyst particles," Chem. Eng. Res. Des. **81**, 953–962 (2003).